Supplementary Information

I. Simulation of heat transfer characteristics in the device

Numerical simulations were performed with COMSOL Multiphysics (Chemical Engineering Module). We employed a 2D model coupling porous channel flow and convection-conduction equations. The flow was described by the Navier-Stokes equation in the media flowing channel and the Brinkman equation in the porous agar gel membrane. The Brinkman equation describes flows in porous media, for which the momentum transport within the membrane due to shear stresses is of importance. These equations extend Darcy's law to include a term that accounts for the viscous transport in the momentum balance and is valid where the porosity is high (i.e. >90%).[1,2]

Flow in the free channel is described by the Navier-Stokes equations:

$$\nabla \cdot \mathbf{u} = 0 \tag{S-1}$$

$$\rho(\mathbf{u} \cdot \nabla)\mathbf{u} = \nabla \cdot \left[-p\mathbf{I} + \eta\left(\nabla\mathbf{u} + (\nabla\mathbf{u})^T\right)\right] \tag{S-2}$$

where η denote the dynamic viscosity of the fluid (kg m/s), $\mathbf{u}$ is the velocity vector (m/s), ρ is the density of the fluid (kg/m^3), p is the pressure (Pa). In porous medium, the Brinkman equations are described as

$$\nabla \cdot \mathbf{u} = 0 \tag{S-3}$$

$$\frac{\eta}{\kappa}\mathbf{u} = \nabla \cdot \left[-p\mathbf{I} + \frac{\eta}{\varepsilon}\left(\nabla\mathbf{u} + (\nabla\mathbf{u})^T\right)\right] \tag{S-4}$$

where ε is the porosity, and κ is the permeability of the porous medium (m^2). Physical properties used in the modeling are listed in Table S1. The velocity profiles across the flowing media and agar membrane subdomains (Figure S1 (a)) are depicted in Figure S1 (b). Due to relatively low permeability of the agar membrane, velocities in the agar membrane under all flow media velocities are negligible, in the order of 10^{-7} m/s, compared to 10^{-3} m/s in the media flow channel.

Heat transfer properties of the device are modeled with transient convection-conduction equation as

$$\rho C\left(\frac{\partial T}{\partial t}+\mathbf{u}\nabla\cdot T\right)=\nabla\cdot\left(k\nabla T\right) \tag{S-5}$$

where k denote the thermal conductivity (kg/ms) and C is the heat capacity(J/kgK). Initial conditions of all boundaries are 25 °C except the bottom of glass slide (colored red in Figure S1 (a)) which is maintained at specified temperature as heat source.

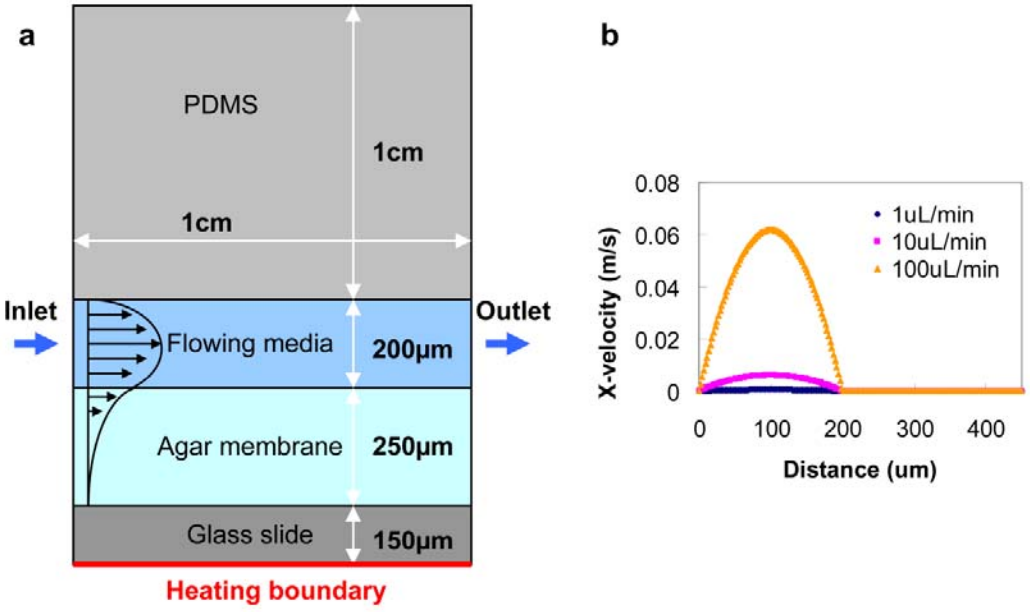

Figure S1. Illustrative and geometrical depiction of the simulation model using COMSOL. **(a)** Media only flow from the inlet to the outlet. Bottom of the glass slide (colored red) is a constant temperature boundary maintained at specified temperature. Initial conditions of all other subdomains were set at 25 °C. (b) Velocity profiles across the fluid flow-active subdomains (flowing media and agar membrane) at different flow rate. Negligible velocity in agar membrane subdomain is calculated due to the low permeability of the agar membrane.

Table S1. Physical constants used in the simulation.

Description	Material	Value
Thermal conductivity k (W/m·K)	PDMS	0.15[5]
	Water	0.611
	Glass	1.13
	1.5% Agar	0.6[5]
Density ρ (kg/m^3)	PDMS	970[6]
	Water	1000
	Glass	2235
	1.5% Agar	1000[5]
Heat capacity C (J/kg·K)	PDMS	1500[6]
	Water	4216
	Glass	710
	1.5% Agar	3900[5]
Dynamic viscosity η (Pa·s)	Water	0.001
	1.5% Agar	0.001
Porosity ε	1.5% Agar	0.9854[7]
Permeability κ	1.5% Agar	2816e-18[7, 8]

II. Image analysis software – Bacteria Tracking

Bacteria Tracking is an application for interactive tracking of bacteria samples and collecting their fluorescent intensity data. It is written in an open source programming language and environment called *Processing*. Processing consists of the Processing Development Environment, a collection of built-in functions and external libraries that are contributed by the community. It is a cross-platform and based on the graphical capabilities of the Java programming language, which make it an ideal tool for visualizing data, analyzing images and creating user-interfaces. The Bacteria Tracking program consists of four major modules: i. image acquisition, ii. user interface, iii. image processing, and iv. data collection and storage.

Before the image and data are loaded to the Bacteria Tracking program, they are organized and prepared in ImageJ which is used to select and crop the whole stack of images to smaller pieces. Two types of image/data are generated using ImageJ: i. bright-field or flattened fluorescence images-stacks - for visualization and cell tracking and saved as jpeg formats; ii. Fluorescent data images-stacks of different color channels - the fluorescent intensity values in every pixel is extracted and stored as text files. The Bacteria Tracking program starts with loading the sequence of bright-field and fluorescence image files. The program displays the cell tracking image stacks. Tracking processing starts from the last image and traces backward to the first image to avoid ambiguity in identifying bacteria correspondence during cell division. Bacteria edges are detected semi-automatically by using the average threshold level of each bacterial cell, which greatly saves the time in manually drawing region on each bacterial cell (Figure S2).

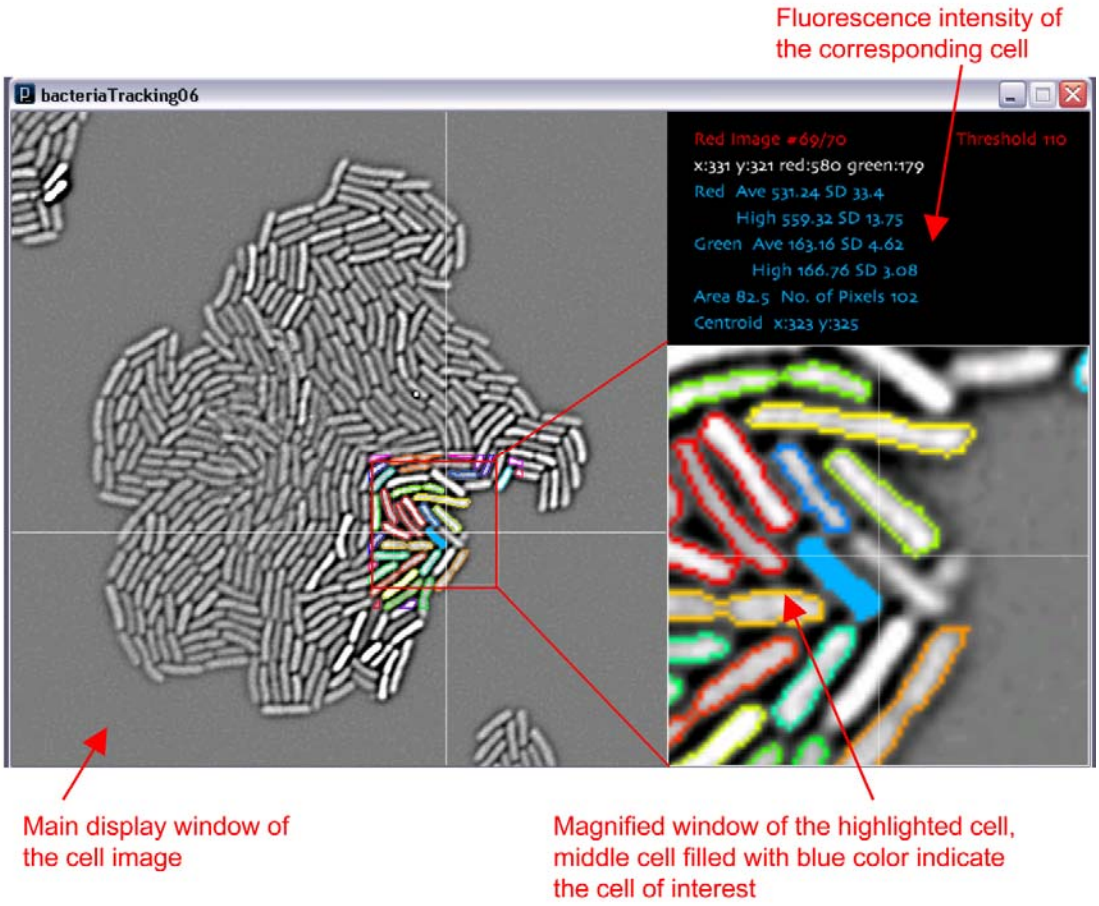

Figure S2. A snapshot of Bacteria Tracking software in use. Top right: Display of image data including cell centroid coordinates, cell area, number of pixels of the cell, and fluorescence signals of the cell in the corresponding time frame. Bottom right bottom: magnified window of the highlighted cells, middle cell filled with blue color indicate the cell of interest.

III. Cell strains

Gene-Metabolic oscillator. The basic concept of this metabolic oscillator is similar to the previous study.[3] Detailed description of the constructs is described in a separate publication.[4] M9 media cultures with 1% glucose grown with antibiotics (30μg/ml Kanamycin and 100μg/ml Ampicillin). Isopropyl-b-D-thiogalactoside (IPTG) was added into the media to switch on the oscillation machinery.

Ethanol induced uspA-RFP expression. UspA promoter was amplified with primers HW9F and HW9R from *E. coli* BW25113 WT genomic DNA. Mcherry gene was amplified with primers HW10F and HW10R from *E. coli* DH5. Z1 contains pZE12-mcherry plasmid. These two DNA fragments were fused by splicing and overlapping extension PCR. The resulting PCR product was digested with *Xho*I and *Hind*III and subsequently cloned into pCS19 between the same pair of restriction sites, creating pHW3 plasmid and transformed into JCL260.

Primer sequence:

HW9F	GGCCG CTCGAG TTTATCTAACGAGTAAGCAA
HW9R	ATGAACTCCTTGATGATGGCCATGTTATCCTCCTCGCCCTTGCT CACCATAGTGTTACTCCTTCCATAAA
HW10F	ATGGTGAGCAAGGGCGAGGA
HW10R	CCGAAGCTTTTACTTGTACAGCTCGTCCA

Isobutanol tolerant cell. The high isobutanol tolerance (HTS) and refrence strains (RS) were obtained from the laboratory of Professor James C. Liao, University of California, Los Angeles.

LVA-tagged GFP strain. $GTP_{mut3.1\text{-}LVA}$ was cloned into pZE12-luc between *Acc65I* and *XbaI* restriction sites through PCR cloning, with the degradation sequence flanked at the end of the reverse primer and transformed into DH5αZ1.

IV. Repeated experiments for cell proliferation

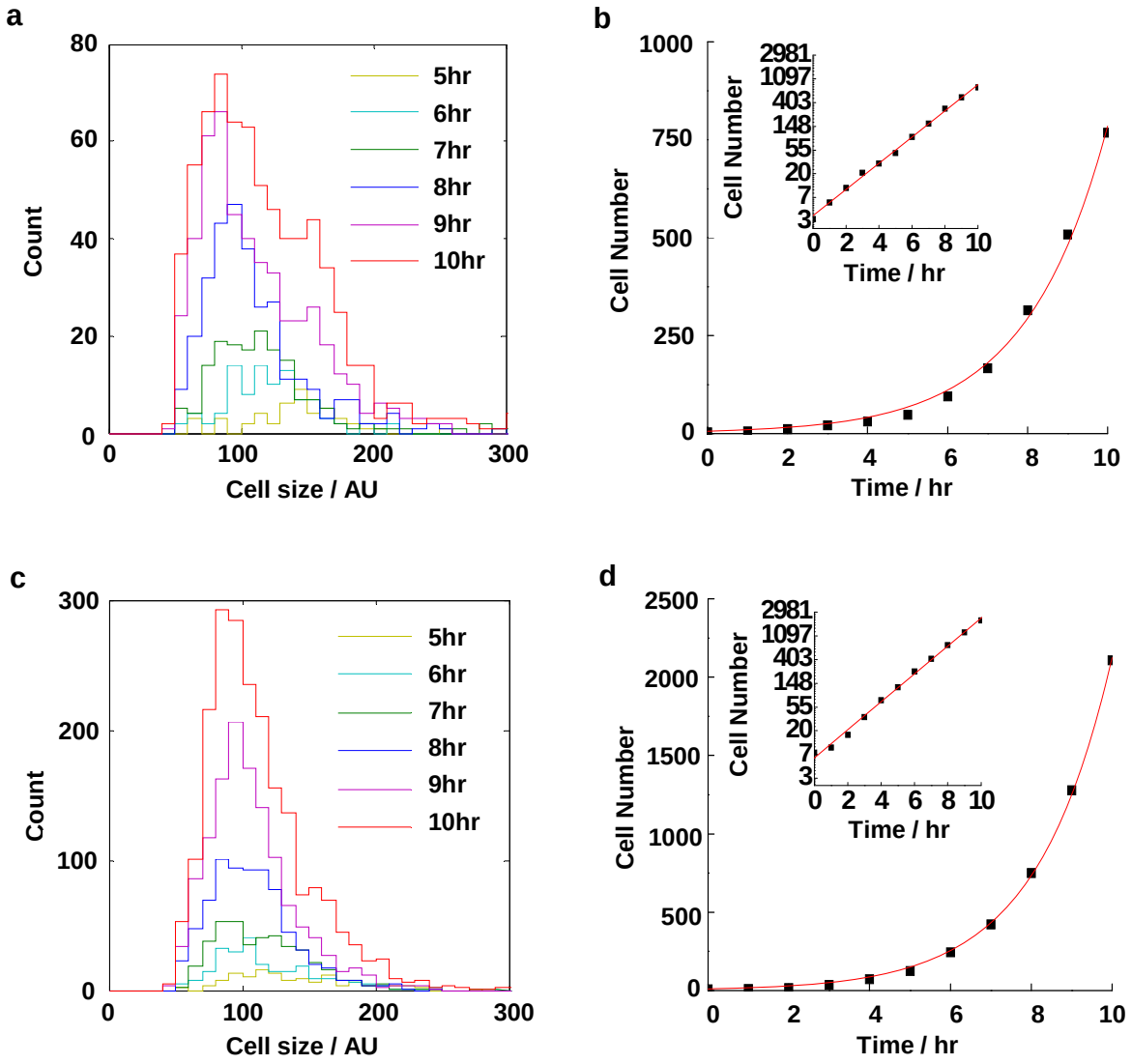

Figure S3. Repeated Experiments of cell proliferation. Experiment set 1: (a) Histograms of cell sizes measured at various time points, (b) Colonies growth curve, specific growth rate is 0.55283. Experiment set 2: (c) Histograms of cell sizes measured at various time points, (d) Colonies growth curve, Specific growth rate is 0.58883. The specific growth rate of the experiment in Figure 2 is 0.57977.

V. Dynamic chemical environment control

We examined the dynamic chemical environment control feasibility of our device using bacterial cells carrying GFP plasmids tagged with LVA degradation tag (GFP-LVA), expressed under an IPTG-inducible promoter. This GFP variant has a short half-life in bacteria due to the presence of the C-terminal tail that targets the protein for degradation by specific bacterial proteases.[9] In the experiment, we switched between 2 types of M9 media containing either 1 mM and 0 mM of IPTG (both containing glucose and supplements) with either 1-hr and 2-hr cycle (Figure S4 and Movie S2 and S3). Cell experiments were carried out as described in Experimental and Methods section in the manuscript. Strain construction can be found in Supplementary Information part III.

The results showed that GFP signal followed well with the IPTG +/- infusion cycle. Fluorescence level of the 2-hr cycle experiment is generally higher than that of the 1-hr cycle experiment, mainly because of the longer time in the former case allowed for bacteria to produce GFP during the IPTG+ period. It can also be noted, in both 1 hr and 2 hr cycle experiments, that the lag time for GFP signal to rise (~10min) is approximately one time shorter than the lag time for GFP signal to drop (~20min). This is in accordance to our fluorescein diffusion characterization which shows that the time for fluorescein to diffuse out is slower than the rate of fluorescein to diffuse into the membrane (Figure 3c). The 10 min lag time includes the time needed for protein synthesis ranging from ~ 5 to 10 min. Moreover, as can be noticed from the Supplementary Movies S2 and S3, there are increasing number of cells exhibiting incomplete fluorescence level drop to the base level. This mainly arose from the nature of stochastic distribution of cellular materials upon cell division, leading to uneven protein degradation rate.

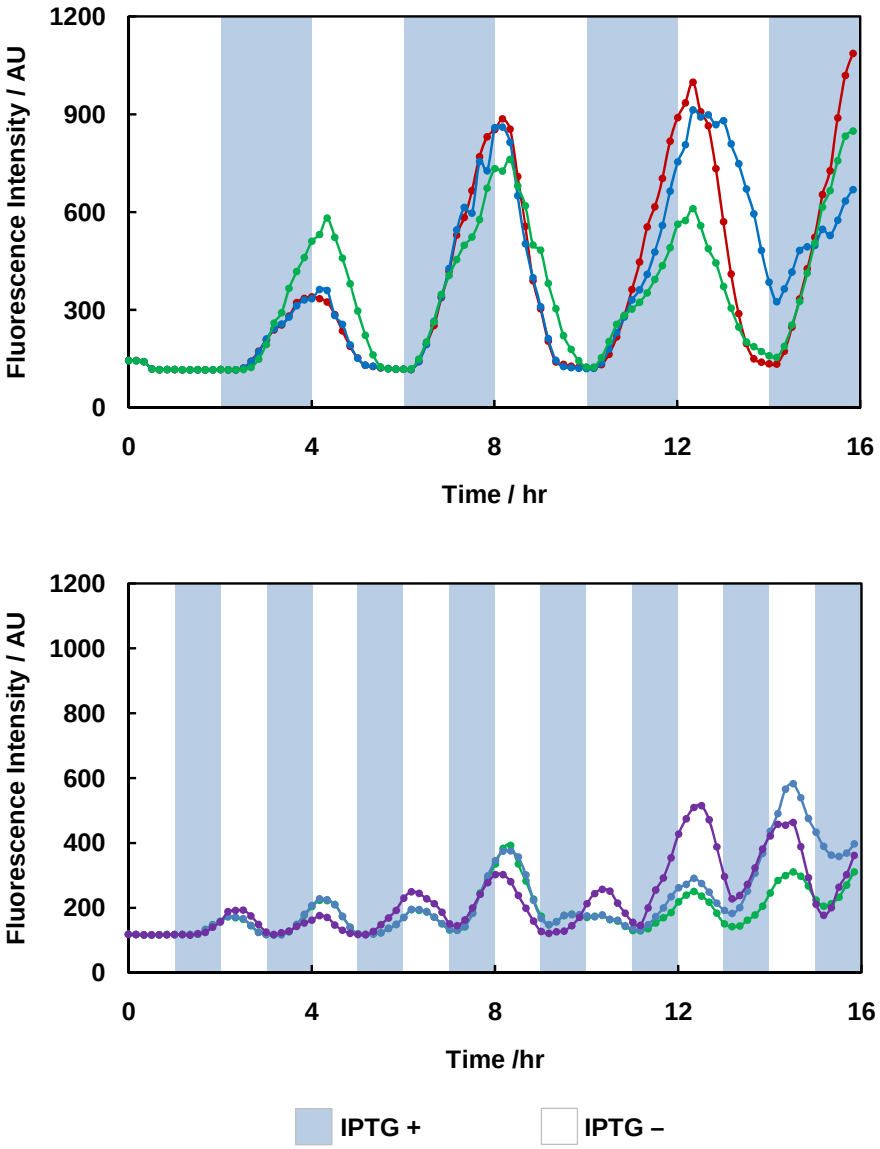

Figure S4. Representative long term single cell GFP fluorescence tracking in dynamically switched chemical environments containing either 1 mM or 0 mM of IPTG. Media were infused to the microchannel at 10 μL min^{-1} with temperature maintained at 30 °C. Fluorescence intensities of single cell were captured every 10 min. Blue colored bar indicates media containing 1 mM IPTG and white colored bar indicates media containing 0 mM IPTG. Top: 2 hr cycle. Bottom: 1 hr cycle. 3 individual cells were tracked for each cycled experiments.

References

1 M. Parvazinia, V. Nassehi, R. Wakeman and M. Ghoreishy, *Transp. in Porous Media*, 2006, **63**, 71-90.
2 H. Brinkman, *Appl. Sci. Res.*, 1949, **1**, 27-34.
3 E. Fung, W. W. Wong, J. K. Suen, T. Bulter, S. G. Lee and J. C. Liao, *Nature*, 2005, **435**, 118-122.
4 H. Taizo, A. Atsumi and J. C. Liao, unpublished work.
5 O. K. Bates, *Ind. Eng. Chem.*, 1949, **41**, 1966-1968.
6 A. Elliott, J. Schwartz, J. Wang, A. Shetty, J. Hazle and J. R. Stafford, *Lasers Surg. Med.*, 2008, **40**, 660-665.
7 W. Y. Gu, H. Yao, C. Y. Huang and H. S. Cheung, *J. Biomech,*, 2003, **36**, 593-598.
8 M. E. Johnson and M. W. Deen, *AIChE J.,* 1996, **42**, 1220-1224.
9 J.B. Anderson, C. Sternberg, L.K. Poulsen, S.P. Bjorn, M. Givskov, S. Molin, *Appl. Environ. Microbiol.* **64**, 2240-2246.